Parenchymal texture analysis in digital mammography: A fully automated pipeline for breast cancer risk assessment

Yuanjie Zheng, Brad M. Keller, Shonket Ray, Yan Wang, Emily F. Conant, James C. Gee, and Despina Kontos[a)]
Department of Radiology, Perelman School of Medicine, University of Pennsylvania, 3600 Market Street, Suite 370, Philadelphia, Pennsylvania 19104

(Received 13 December 2014; revised 5 May 2015; accepted for publication 13 May 2015; published 16 June 2015)

Purpose: Mammographic percent density (PD%) is known to be a strong risk factor for breast cancer. Recent studies also suggest that parenchymal texture features, which are more granular descriptors of the parenchymal pattern, can provide additional information about breast cancer risk. To date, most studies have measured mammographic texture within selected regions of interest (ROIs) in the breast, which cannot adequately capture the complexity of the parenchymal pattern throughout the whole breast. To better characterize patterns of the parenchymal tissue, the authors have developed a fully automated software pipeline based on a novel lattice-based strategy to extract a range of parenchymal texture features from the entire breast region.
Methods: Digital mammograms from 106 cases with 318 age-matched controls were retrospectively analyzed. The lattice-based approach is based on a regular grid virtually overlaid on each mammographic image. Texture features are computed from the intersection (i.e., lattice) points of the grid lines within the breast, using a local window centered at each lattice point. Using this strategy, a range of statistical (gray-level histogram, co-occurrence, and run-length) and structural (edge-enhancing, local binary pattern, and fractal dimension) features are extracted. To cover the entire breast, the size of the local window for feature extraction is set equal to the lattice grid spacing and optimized experimentally by evaluating different windows sizes. The association between their lattice-based texture features and breast cancer was evaluated using logistic regression with leave-one-out cross validation and further compared to that of breast PD% and commonly used single-ROI texture features extracted from the retroareolar or the central breast region. Classification performance was evaluated using the area under the curve (AUC) of the receiver operating characteristic (ROC). DeLong's test was used to compare the different ROCs in terms of AUC performance.
Results: The average univariate performance of the lattice-based features is higher when extracted from smaller than larger window sizes. While not every individual texture feature is superior to breast PD% (AUC: 0.59, STD: 0.03), their combination in multivariate analysis has significantly better performance (AUC: 0.85, STD: 0.02, $p < 0.001$). The lattice-based texture features also outperform the single-ROI texture features when extracted from the retroareolar or the central breast region (AUC: 0.60–0.74, STD: 0.03). Adding breast PD% does not make a significant performance improvement to the lattice-based texture features or the single-ROI features ($p > 0.05$).
Conclusions: The proposed lattice-based strategy for mammographic texture analysis enables to characterize the parenchymal pattern over the entire breast. As such, these features provide richer information compared to currently used descriptors and may ultimately improve breast cancer risk assessment. Larger studies are warranted to validate these findings and also compare to standard demographic and reproductive risk factors. [http://dx.doi.org/10.1118/1.4921996]

Key words: digital mammography, parenchymal texture, breast density, cancer risk

1. INTRODUCTION

Breast cancer is the most commonly diagnosed cancer among women and ranks second among cancer related mortality for women in the United States.[1] Among the various imaging modalities, mammography is currently the main choice for screening of breast cancer. Screen-film mammography (SFM) is increasingly being replaced by full-field digital mammography (FFDM), both for screening and surveillance of asymptomatic women as well as in the diagnostic workup of those suspected of malignancies. FFDM offers several potential benefits compared to SFM,[2] including the ability to digitally store and quantitatively analyze the acquired images.[3–5]

Starting with the pioneering work of Wolfe,[6,7] studies have long suggested a relationship between mammographic parenchymal patterns and breast cancer risk.[8–11] These parenchymal patterns are formed by the distribution of fatty, fibroglandular, and stromal breast tissues. An increasingly supported hypothesis is that inherent biological factors, such

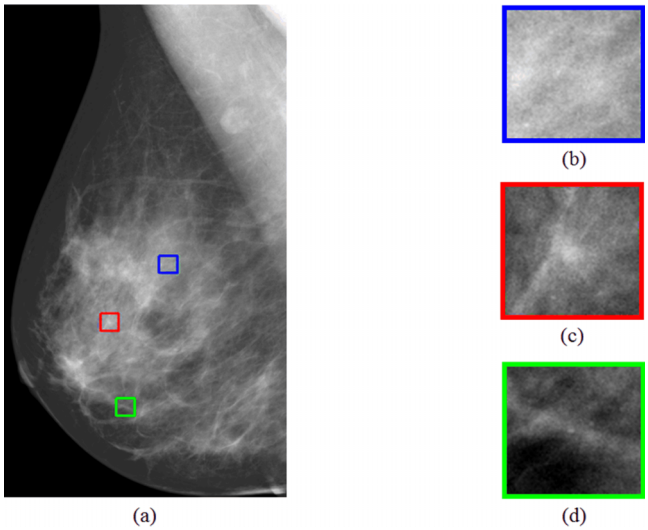

FIG. 1. (a) A digital mammogram of a woman diagnosed with unilateral breast cancer, overlaid with three local ROI windows. (b)–(d): large views of the three local windows (size: 6.3×6.3 mm^2). These views demonstrate the locally heterogeneous properties of the breast tissue.

as endogenous hormonal exposure and genetic predisposition that are associated with the risk of breast cancer, are expressed in a woman's parenchymal tissue and subsequently manifested in her mammographic parenchymal patterns.[12–14]

Currently, the most commonly used descriptor to quantify such parenchymal patterns is breast percent density (PD%), which measures the overall relative amount of fibroglandular tissue in the breast. Breast density has been consistently identified as one of the strongest risk factors for breast cancer.[15] It can be evaluated via visual categorical assessment,[14] such as by using the Boyd or ACR-BIRADS scale, or by using computer-aided methods to estimate a continuous measure of breast PD%.[16–20]

Given that the distribution of dense tissue within the breast is not uniform, there is increasing interest in also measuring the heterogeneity of the parenchymal pattern (Fig. 1) in more granular ways than the global assessment of breast PD%. For example, as described in the early work of Wolfe,[6] the distribution and prominence of ducts were hypothesized to play a role in risk. This empirical observation was later extended to the application of comprehensive categorical descriptors of density patterns in cancer risk assessment.[21] More recently, quantitative characterization of parenchymal patterns with texture features has also attracted research interest.[22] Studies have shown that mammographic texture features are independently related to breast cancer risk[9,11,22–24] and may provide additional information to breast PD%.[25,26]

Most studies to date have computed parenchymal texture features from a single region-of-interest (ROI) which is typically manually placed in the breast (i.e., Fig. 2) in either the retroareolar area,[25] the central breast area,[11,23] the largest rectangular box inscribed within the breast,[27] or as a single feature from the entire segmented breast.[28] However, such approaches may be limited, as they cannot fully capture the granularity and heterogeneity of the parenchymal texture. Following the original definition of image texture,[29–32] mammographic texture should be described as repeated local primitives (i.e., structure elements) estimated over the entire breast. In contrast, most previous approaches either treat such local primitives as the only ROI, ignoring any information outside that ROI [Figs. 2(a) and 2(b)], or estimate these features at a very global level, reducing the granularity of these descriptors.

We hypothesize that the association of mammographic textural measurements and breast cancer risk can be improved if richer texture descriptors are extracted to better characterize the heterogeneity of the parenchymal tissue. We have, therefore, developed a fully automated software pipeline that incorporates a lattice-based strategy to extract a wide range of texture features using adjacent local windows (i.e., primitive

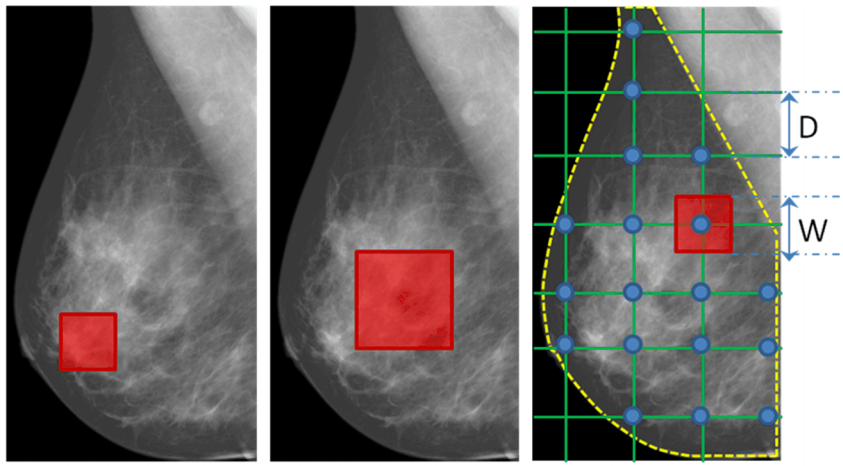

FIG. 2. Single-ROI analysis (a) and (b) allows to characterize parenchymal texture only within a specific tissue region, while a lattice-based strategy (c) can combine a range of local tissue texture features obtained within a window (i.e., the red rectangle with size of W) surrounding each lattice point (i.e., the blue intersection points on the regular grid drawn using green lines), to better characterize the parenchymal tissue heterogeneity within the entire breast (outlined with the yellow dashed curves).

elements) that cover the entire breast. Using a case-control study with digital mammograms, we further examine associations between these lattice-based texture measures and breast cancer, compared to single-ROI texture features and breast PD%. As such, our study serves as a preliminary evaluation of the ability of our lattice-based texture features to predict breast cancer risk. Upon further validation, our proposed texture features could ultimately be incorporated into current breast cancer risk assessment models to improve their discriminatory capacity at the individual level.

2. MATERIALS AND METHODS

2.A. Pipeline overview

Our pipeline is currently implemented to analyze digital mammograms.[33,34] First, the pipeline performs preprocessing steps to segment the breast region followed by z-score normalization of the gray-level intensity values within the segmented breast. Subsequently, breast PD% is estimated using a previously validated automated technique[18] and a set of lattice-based parenchymal texture features is extracted. A logistic regression classifier is then trained using cross validation, by selecting features that most significantly contribute to case-control classification (Fig. 3).

2.B. Preprocessing

The breast region is first segmented using a previously validated algorithm[18] prior to any subsequent texture analysis. Briefly, the air-breast boundary is delineated using automated thresholding.[18] Then, for medio–lateral oblique (MLO) images, the region of the pectoral muscle is removed by identifying its boundary using a straight line Hough transform. Z-score normalization[18] is further applied within the segmented breast region, to standardize gray-level intensity range for all images across subjects.

2.C. Breast density analysis

Different image segmentation techniques have been proposed for estimating breast PD%.[18,35] Here, we used a recently developed method, validated for digital mammography.[18] Specifically, an adaptive multiclass fuzzy c-means clustering algorithm is applied to partition the breast area into a set of subregions with similar image intensity properties. Then, a linear support vector machine classifier labels each of these detected subregions as either being composed primarily of dense tissue or fat. From these labels, breast PD% is estimated as the percentage of the total breast area occupied by the clustered regions of dense (i.e., fibroglandular) tissue.[18]

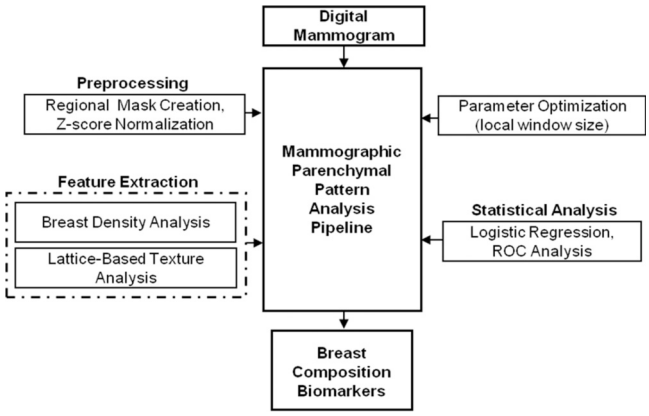

FIG. 3. Flowchart of our fully automated software pipeline for parenchymal texture analysis.

2.D. Texture analysis

2.D.1. Lattice-based strategy

Our lattice-based strategy for computing mammographic texture features is based on a regular grid virtually overlaid on the mammographic image (Fig. 2). This regular grid is specified by vertical grid spacing, represented by "D," which also equals the horizontal spacing. Based on this lattice, texture features are computed for the intersection points (i.e., lattice points) of the grid lines within the breast and this computation is performed inside a local square window of size "W" centered at each lattice point. For each texture descriptor, this strategy results in a texture map which is formed by the texture values computed at each lattice point throughout the breast. In Fig. 4, we show representative texture maps generated by our pipeline.

This lattice-based framework has two main adjustable parameters in computing the texture features. One is the grid spacing D, for which larger values generate fewer lattice points, resulting in a coarser texture map of a smaller scale, and vice versa. The other is the size W of the local window for computing the texture features, which is important for characterizing the locality of the texture pattern and, in principal, is optimal when equal to the size of the local primitive of the intrinsic parenchymal texture structure.

Changing the values of D and W may result in performance differences for the texture features. Due to the heterogeneity of the parenchymal pattern (i.e., Fig. 1), the optimal values of D and W may vary for different locations in the breast. However, for simplicity purposes, here, we assume an equal window size W across the breast, the value of which is optimized experimentally. Furthermore, we assume that D and W have the same value, so that the entire breast region is covered by adjacent windows.

2.D.2. Texture features

We characterize the textural properties of the breast tissue by using two broad types of features (Table I), namely, features estimating statistics of the gray-level histogram in different orders[31,36–38] and structural features describing the architectural composition of the tissue using well-defined elements.[22,39–43] These features have been previously used, primarily in studies with screen-film mammography and single-ROI approaches, for parenchymal tissue analysis in breast cancer risk assessment.[44] We have also previously validated the robustness of these features for different

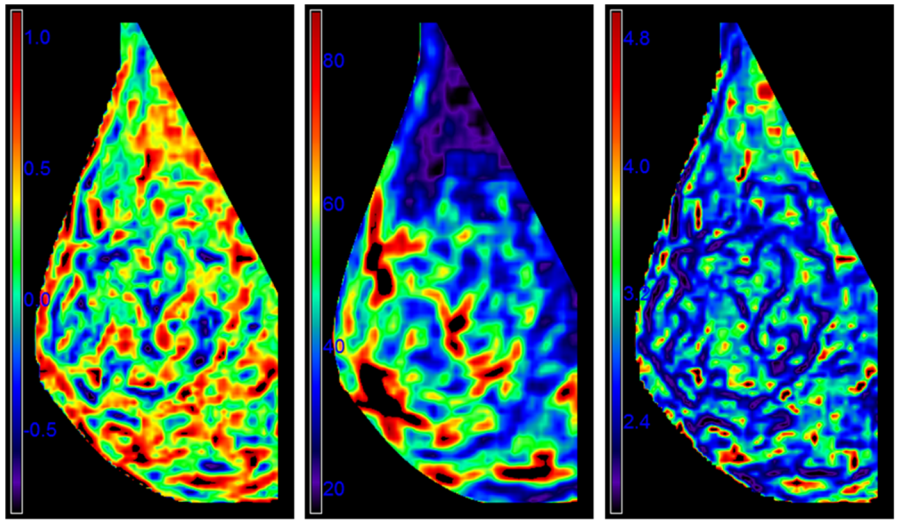

FIG. 4. Illustration of the texture maps concept generated using our lattice-based strategy ($D = W = 11$).

digital mammography detectors, using a statistical feature normalization framework.[45–47]

Statistical texture features cover first-, second-, and higher-order statistics of the image. Specifically, first-order features are calculated from the gray-level intensity histogram and include estimates of the mean, variance, skewness, kurtosis, gray-level percentile (i.e., a measure of the shape of the gray-level histogram), and entropy.[36] While first-order statistics consider only the pixels' intensities, second-order statistics are based on gray-level co-occurrence matrices (GLCMs) and also consider the spatial relationships of pixels. A co-occurrence matrix measures the probability that a pixel of a certain gray-level intensity appears at a specific distance and orientation from a pixel of another given intensity.[37] Finally, higher-order statistics include run-length measures, which describe texture by measuring "runs" of consecutive pixels with similar gray levels and calculate statistics based on the number and length of such runs.[38] As such, long runs of the same gray-level value correspond to coarser textures, whereas shorter runs correspond to finer textures. The structural features include fractal dimension as estimated by the box-counting method,[22,39,40,48] the local binary pattern (LBP)[41] which captures intensity variations between central and neighboring pixels, and the edge-enhancing index feature[42,43] which describes the directionality of flow-like structures within the breast. In summary, a total of 30 texture features are incorporated in our pipeline and used in our subsequent analysis (Table I, the Appendix).

For our experiments, related parameters for feature extraction were based on our preliminary studies[33,34,45] and previous related published literature[22,31,36–41,43] in which these parameters were optimized. For the image histogram-based features, the number of histogram bins was set to 128. Co-occurrence matrix-based features were computed by using the same offset length of 11 pixels (1.1 mm) and averaging along four directions (0°, 45°, 90°, and 135°), based on the premise that these features are orientation invariant. For computing LBP, the neighborhood size and the number of neighboring pixels were set to three pairs: (1,8), (2,20), and (3,36), respectively. For computing the edge-enhancing index feature, the size of the Gaussian kernel to smooth each image was set to 1, 5, 10, and 15 pixels (0.1, 0.5, 1.0, and 1.5 mm),

TABLE I. List of texture features incorporated in our pipeline and used for parenchymal pattern analysis.

Feature type		Feature name
Statistical	Gray-level histogram	Max, min, mean, sum, entropy, kurtosis, sigma, skewness, 5th, 5th mean, 95th percentile, 95th mean
	Co-occurrence	Cluster shade, energy, entropy, inertia, correlation, Haralick correlation, inverse difference moment
	Run-length	Gray-level nonuniformity, high gray-level run emphasis, low gray-level run emphasis
Structural	Edge-enhancing index	Radius-1 edge center, radius-5 edge center, radius-10 edge center, radius-15 edge center
	Local binary pattern	Radius-1 LBP center, radius-2 LBP center, radius-3 LBP center
	Fractal dimension	Box-counting fractal dimension

respectively, and for each of them, the computed edge center was treated as an independent feature as shown in Table I. To determine the optimal local window size for texture feature extraction (i.e., the lattice window of size W), we tested different window sizes W of 63, 127, and 255 pixels (6.3, 12.7, and 25.5 mm, respectively).

2.E. Pipeline evaluation

2.E.1. Image acquisition and study data

We retrospectively analyzed raw (i.e., "for processing") MLO view digital mammograms, under HIPAA and IRB approvals. The cases included women diagnosed with biopsy-proven unilateral primary invasive breast cancer ($n = 106$). All cases were collected from a multimodality breast imaging trial previously completed at our institution during 2002–2006 (NIH P01 CA85484, "Evaluation of Multimodality Breast Imaging"; PI: M. D. Schnall). Their breast density distribution was 3.8%, 47.2%, 48%, and 1% for BIRADS categories 1, 2, 3, and 4, respectively. The contralateral images (i.e., from the unaffected breast) were analyzed, as a surrogate of inherent breast tissue properties predisposing these women to a higher risk of breast cancer.[25] Controls were randomly selected from the pool of women with negative screening mammograms at same time-period in our institution and age-matched to cases based on 5-year intervals at a (3:1) ratio ($n = 318$). Their BIRADS density distribution was equal to 6.6%, 41.5%, 50.6%, and 1.3% for the same corresponding categories. Their raw images were side-matched to cases, resulting in a total of 424 digital mammograms included in our analysis. All images were acquired using either a GE Senographe 2000D or DS digital mammography system (GE Healthcare, Chalfont St Giles UK), with 14-bit pixel gray-level depth and 10 pixel/mm resolution.

2.E.2. Classification experiments

The association between our lattice-based texture features and breast cancer was evaluated using logistic regression analysis with leave-one-out cross validation[49] and incremental forward feature selection.[50] To maintain the age-matched study design during cross validation, each leave-one-out loop is carried out as treating one cancer case and its three age-matched controls as the test set while all other samples are used for training. This is repeated such that all subjects have been chosen one time for testing. For each texture descriptor, the mean of the corresponding texture values over all lattice points within the breast was estimated and used as an input to the classifiers. Both univariate and multivariate analyses were performed. For multivariate analysis, feature selection was performed independently within each leave-one-out loop, and the corresponding frequency of selection was recorded for all features. We evaluated feature performance for the different values of the local window size W, and compared against the performance of the same texture features when extracted as previously proposed from a single-ROI in the retroareolar[25] or the central breast region.[11,23] Finally, we investigated the performance and added value of our lattice-based texture features as compared to standard breast PD%. The area under the curve (AUC) of the receiver operating characteristic (ROC) was used as a performance metric, as estimated by the ROCKIT algorithm (WINDOWS version 1.0.1 BETA 2).[51] Statistical significance of the AUCs was assessed in comparison to a random guess (AUC = 0.50), and differences when comparing the different AUCs obtained were estimated using the DeLong's test.[52] No explicit correction was applied for multiple comparisons.

3. RESULTS

3.A. Univariate performance

Overall, the average cross-validated performance of the co-occurrence features over all window sizes (AUC_{avg}: 0.58, AUC_{std}: 0.03, $p < 0.05$) is better than the performance of the gray-level histogram (AUC_{avg}: 0.56, AUC_{std}: 0.05, $p > 0.05$), run-length (AUC_{avg}: 0.56, AUC_{std}: 0.05, $p > 0.05$), and structural features (AUC_{avg}: 0.57, AUC_{std}: 0.06, $p > 0.05$) (Fig. 5). The performance over all categories of texture features also appears to be on average higher for smaller window sizes, where the window size W of 63 pixels (AUC_{avg}: 0.58, AUC_{std}: 0.07, $p < 0.05$) performs better than 127 pixels (AUC_{avg}: 0.57, AUC_{std}: 0.05, $p > 0.05$) or 255 pixels (AUC_{avg}: 0.54, AUC_{std}: 0.03, $p > 0.05$). The best performing texture feature is "fractal dimension" for a window size W of 127 pixels (AUC: 0.69, STD: 0.03, $p < 0.05$) and 63 pixels (AUC: 0.69, STD: 0.03, $p < 0.05$), and they both significantly outperform PD% (AUC: 0.59, STD: 0.03, $p < 0.05$). The worst and most unstable performance is observed for the gray-level histogram feature "sum" when using a window size of 255 (AUC: 0.50, STD: 0.03, $p > 0.05$). The AUCs for each of our lattice-based texture features and all different parameter settings are provided in Tables S1–S3 of the supplementary material.[53]

3.B. Multivariate performance

When combining all texture features in a multivariate logistic regression classifier, the lattice-based texture features

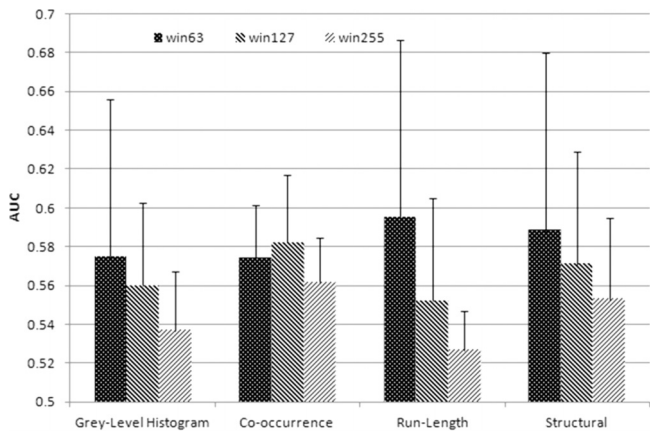

FIG. 5. ROC performance of univariate logistic regression for the lattice-based texture features extracted with different local window sizes. The bar plots show the corresponding average AUC values (with the standard deviation) for each category of texture features.

also perform best when computed from smaller window sizes (Fig. 6), with the window sizes of 63 (AUC: 0.85, STD: 0.02), outperforming the window sizes of 127 (AUC: 0.81, STD: 0.02, $p > 0.05$) and 255 pixels (AUC: 0.76, STD: 0.03, $p < 0.01$). Regardless of which window size the lattice-based texture features are computed, they consistently and significantly outperform breast PD% (AUC: 0.59, STD: 0.03, $p < 0.001$). No appreciable improvement ($p > 0.05$) is obtained by adding PD% to the lattice-based texture features for any window size, compared to the multivariate performance of the lattice-based texture features alone (Fig. 6).

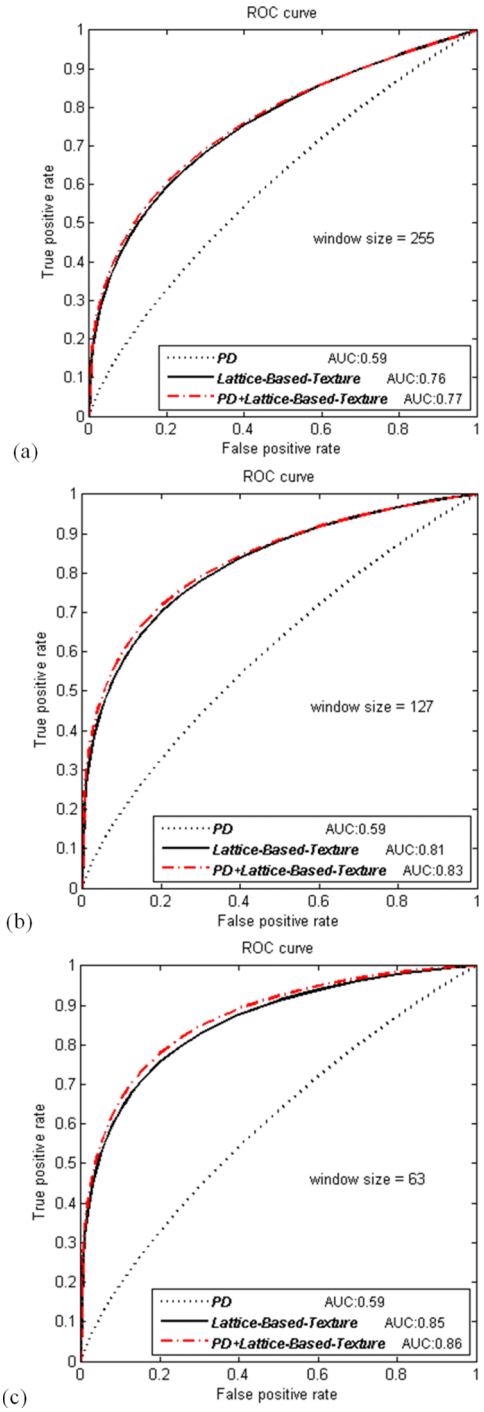

FIG. 6. Case-control classification performance for PD% (dotted line), lattice-based texture features for windows (a) 255, (b) 127, (c) 63 (continuous line), and PD% plus texture features (dot-dash red line).

Table II shows the features ranked as selected by incremental forward selection for the best performing window size of 63 pixels (6.3 mm). Overall, fractal dimension, run-length, co-occurrence, and gray-level histogram features are more frequently selected than the local binary and edge-enhancing index features by the classifier.

Compared to single-ROI based approaches [Fig. 7(a)], our lattice-based texture features significantly outperform ($p < 0.001$) the same texture features when extracted from the retroareolar[25] (AUC: 0.60, STD: 0.03) or the central breast area[11,23] (AUC: 0.74, STD: 0.03). This performance improvement also holds when combining with PD% [Fig. 7(b)], as the lattice-based texture features still significantly outperform ($p < 0.001$) the single-ROI features from the retroareolar (AUC: 0.64, STD: 0.03) and the central breast area (AUC: 0.75, STD: 0.03). Breast PD% does not add value either to the single-ROI based texture features or the lattice-based texture features ($p > 0.05$). The single-ROI texture features from the central area of the breast perform overall better than the retroareolar texture features.

4. DISCUSSION

The radiographic appearance of the breast tissue is increasingly being recognized as a strong breast cancer risk factor.[54] Wolfe originally defined four parenchymal patterns,[6] ranging from lower to higher parenchymal tissue complexity, as related to breast cancer risk. However, most current approaches to quantify parenchymal patterns are limited in their ability to characterize the complexity of the parenchymal tissue. Breast PD% is a rather simplified descriptor, estimated as the percentage of the dense tissue over the total breast area.[16–18] Although consistently shown to have a strong association with breast cancer, breast density has not yet shown the ability to substantially improve the discriminatory performance of current breast cancer risk prediction models.[55] Therefore, a strategy to improve breast cancer risk assessment could be to incorporate richer descriptors of the parenchymal pattern complexity.

There are two principal concepts in most formal definitions of image texture.[29,30,32] First is the notion that a local primitive element exists, which is repeated over a region larger in comparison to the primitive's size. Second, these local primitives are roughly uniform entities having approximately the same dimensions everywhere within the textured region. Therefore, according to these principles, texture features should first be extracted from a local region with an optimal size, determined by the dimension of the local primitive element, and then statistically and structurally summarized over the entire textured region. A similar idea has also been exploited in a related recent work[56] which characterizes parenchymal texture using textons[30] in order to perform mammographic density segmentation.

Based on this formal definition of image texture, we proposed a lattice-based texture analysis strategy, which not

TABLE II. Feature selection frequencies of the lattice-based texture features for window size $W = 63$, as ranked by incremental forward feature selection over all the leave-one-out classification loops.

Rank	Feature	Score	Rank	Feature	Score
1	Fractal Dimension	1.00	16	Grey-level-histogram-Entropy	0.49
2	Co-occurrence_Entropy	0.98	17	Grey-level-histogram_5th	0.47
3	Co-occurrence_InverseDifferenceMoment	0.94	18	Grey-level-histogram_Max	0.40
4	Run-length_HighGreyLevelRunEmphasis	0.89	19	Edge-Enhancing-Index_Radius_1	0.38
5	Local-Binary-Pattern_Radius_1	0.88	20	Grey-level-histogram_95thMean	0.35
6	Co-occurrence_Correlation	0.77	21	Co-occurrence_ClusterShade	0.31
7	Grey-level-histogram_Min	0.76	22	Grey-level-histogram_95th	0.28
8	Co-occurrence_Inertia	0.71	23	Edge-Enhancing-Index_Radius_5	0.22
9	Run-length_LowGreyLevelRunEmphasis	0.67	24	Run-length_GreyLevelNonuniformity	0.19
10	Grey-level-histogram_Kurtosis	0.66	25	Edge-Enhancing-Index_Radius_15	0.17
11	Grey-level-histogram_Skewness	0.62	26	Local-Binary-Pattern_Radius_3	0.14
12	Grey-level-histogram_5thMean	0.53	27	Edge-Enhancing-Index_Radius_10	0.13
13	Co-occurrence_HaralickCorrelation	0.51	28	Local-Binary-Pattern_Radius_2	0.07
14	Grey-level-histogram_Sigma	0.51	29	Grey-level-histogram_Mean	0.01
15	Co-occurrence_Energy	0.50	30	Grey-level-histogram_Sum	0.00

only computes texture features in an optimal local fashion but also characterizes the parenchymal pattern over the entire breast. This lattice-based strategy extracts texture features very differently as compared to the conventional breast PD% and single-ROI based approaches[9,11,22,23] (Fig. 2). While breast PD% is a global measure of the relative amount of dense tissue and single-ROI texture features are extracted from a selected breast region, our lattice-based features are computed at each lattice point within the breast, providing more comprehensive descriptors of the intrinsic parenchymal pattern heterogeneity throughout the breast.

Our results indicate certain key findings. First, not all individual texture features generated by the proposed lattice-based strategy are necessarily superior to breast PD%, but it is rather the combination of a set of selected texture features which result into significantly better performance. This suggests that single texture features may not be enough to fully characterize the parenchymal pattern, but a range of optimally selected and combined texture features may be able to better capture heterogeneous characteristics of the intrinsic breast parenchymal tissue pattern. Interestingly, texture features that capture the overall parenchymal pattern structure, such as fractal dimension, entropy, and local binary pattern, appear to be more frequently selected by the classifier compared to intensity-based histogram features, suggesting that intrinsic pattern characteristics may ultimately prove to have more value in assessing breast cancer risk. Second, the size of the local window of the lattice-based strategy plays an important role in the discriminatory capacity of the extracted texture features. Through experiments, we found that the size of 63 pixels (or 6.3 mm) performs best, as compared to larger window sizes, suggesting that smaller window sizes are more appropriate for characterizing the parenchymal pattern. Third, the lattice-based texture features perform significantly better ($p < 0.001$) than the single-ROI based texture features. Breast PD% did not improve the performance of either the lattice-based texture features or the single-ROI texture features. This observation suggests that texture features, when computed with optimized parameters, may ultimately be able to capture the parenchymal pattern information described by breast PD%.

Although a direct comparison cannot be performed, the best AUC value generated by our texture features is 0.85 (Fig. 6) and appears to be higher than the results reported in current literature for similar populations, including the generic texture features used by Haberle *et al.*[28] (AUC: 0.79), the mammographic texture resemblance marker reported by Nielsen *et al.*[8] (AUC: 0.66), and the texture measurements analyzed by Manduca *et al.*[11] (AUC: 0.58). However, it is lower than the fractal features of Li *et al.*[10] (AUC: 0.93) who also included BRCA1/2 carriers in their study. It is worth noting, however, that in our study, we used a relatively simple approach (i.e., the statistical mean) to summarize the lattice-based texture features throughout the breast. As such, it is reasonable to expect that the discriminatory performance of the lattice-based features can be further improved if more advanced dimensionality reduction techniques are used for this purpose, such as principal component analysis,[57] which could retain additional information from the original texture feature image. Therefore, future investigations should also seek to explore the optimal approach for parameterizing the rich information provided by these features.

Certain limitations should also be acknowledged for our study. We used the contralateral mammograms of the cancer cases at the time of diagnosis rather than prospective follow-up. We also primarily evaluated a potential optimization for the window size W, keeping $D = W$ so that the entire breast region would be covered, while in principal, several combinations of these two parameters could be tested, including optimizing the extent of the local primitives of mammographic texture by looking for an optimal local scale of image texture, based on a multiscale analysis process.[58,59]

In addition, we compared our lattice-based texture features to breast density estimates obtained by only one specific algorithm,[18] while several other implementations exist in the literature, including also volumetric density measures.[60] Our

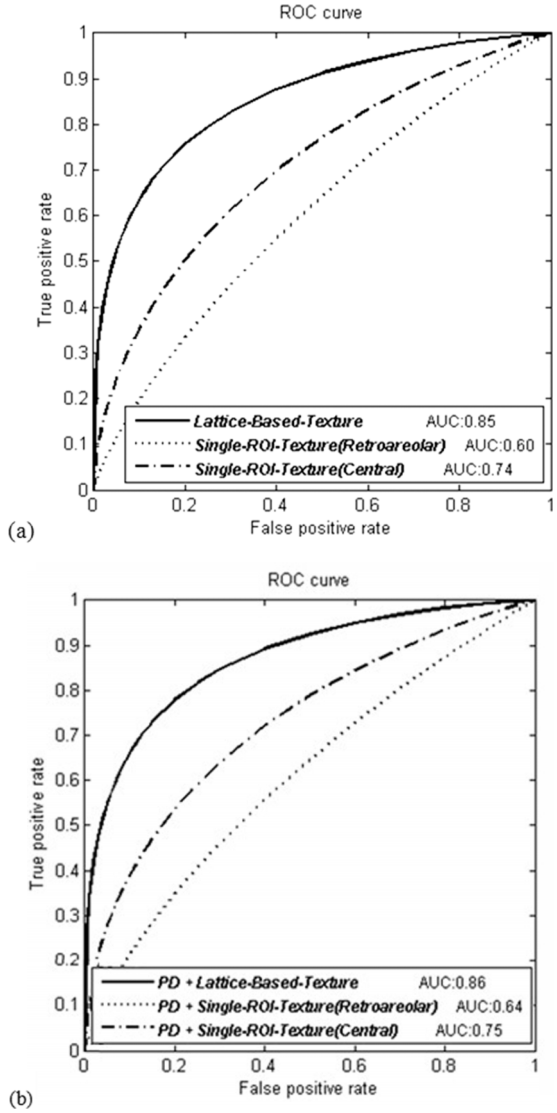

FIG. 7. Case-control classification performance for lattice-based texture features (window size 63) compared to single-ROI texture features (a) without and (b) with the combination of breast PD%.

intention with this study was to show feasibility for our lattice-based strategy for texture analysis and proof-of-concept that our extracted texture features constitute rich descriptors of the parenchymal pattern that may ultimately improve breast cancer risk prediction. Considering the encouraging performance, several other combinations of feature extraction parameters could also be explored in future larger studies.

Of note, for certain features, we observed differences between their univariate versus their multivariate performances after incremental forward feature selection. In our feature selection process, each feature's performance is measured by assuming its range in the two classes of the training samples to follow a Gaussian distribution and then computing the distance between these two distributions. In contrast, in our univariate analysis, each feature performance is measured directly using the AUC of the ROC curve. This difference may, in turn, cause a feature with a lower AUC value in the univariate analysis to be selected more frequently in the feature selection process, or a feature with a higher AUC value to be selected less frequently. As such, our findings will need to be validated prospectively in larger independent populations, including evaluating a broader range of pipeline parameters such as window sizes that vary within the breast or sparser lattice spacing. Ultimately, our features should also be evaluated in conjunction to current standard risk predictors, including demographic and reproductive (i.e., Gail/Claus) risk factors,[61] ethnicity, and BMI, to evaluate their potential added value in breast cancer risk assessment.

5. CONCLUSION

We proposed a fully automated software pipeline for mammographic parenchymal pattern analysis, which uses a lattice-based strategy to extract parenchymal texture features throughout the entire breast region. Using a case-control study, we show that our lattice-based texture features outperform current approaches based on single-ROIs for mammographic texture analysis and standard breast PD%, potentially providing more comprehensive descriptors of the parenchymal pattern complexity for the entire breast tissue. As such, our features may ultimately have complementary value in breast cancer risk assessment. Larger studies are warranted to validate our findings prospectively in independent populations as well as compare to standard risk factors. Additional strategies for further optimizing the parameters of the grid spacing and size of the local square window will also be investigated in these future larger studies.

ACKNOWLEDGMENTS

This work was supported by an American Cancer Society Research Scholar Grant (No. RSGHP-CPHPS-119586) and the National Institutes of Health (Nos. 5R01CA161749-02 and U54CA163313-01). The authors would also like to thank Dr. Mitchell D. Schnall for providing access to the clinical trial data, and Dr. Andrew D. A. Maidment and Ms. Kathleen Thomas for facilitating access to the imaging data included in the analysis.

APPENDIX: TEXTURE FEATURE LIST

1. Gray-level histogram features

Gray-level histogram features characterize the first order statistical properties of the image's histogram. Given an image with intensity $I = (I(i,j))$, dimensions $i = 1,\ldots,M$ and $j = 1,\ldots,N$, the gray-level histogram features evaluated in the paper are listed in Table III.

Entropy describes the amount of randomness within a given image; the higher the entropy the greater the randomness. Kurtosis measures whether the image distribution is peaked or flat relative to a normal distribution. Skewness is a measure of the image histogram's symmetry.

2. Co-occurrence features

Co-occurrence features are a class of features describing the spatial relationship between the pixels, and features are

TABLE III. First order histogram features.

Name	Definition	Name	Definition
Max(:MAX)	$\max_{i,j} I(i,j)$	Kurtosis(:KTS)	$\frac{(I-\bar{I})^4}{(\mathrm{MN}-1)\mathrm{std}(I)^4}$
Min(:MIN)	$\min_{i,j} I(i,j)$	Skewness(:SKEW)	$\frac{(I-\bar{I})^3}{(\mathrm{MN}-1)\mathrm{std}(I)^3}$
Sum(:SUM)	$\sum_{i,j} I(i,j)$	Fifth percentile(:5TH)	$I_{0.05}: \frac{\{p\|I(p)\le I_{0.05}\}}{n_1 n_2} = 5\%$
Mean(:MEAN)	$\bar{I} = \sum_{(i,j)} I(i,j)/\mathrm{MN}$	Fifth mean(:5THM)	$I_{0.05\mathrm{mean}} = \frac{\sum_{I(p)\le I_{0.05}} I(p)}{\|\{p\|I(p)\le I_{0.05}\}\|}$
Standard deviation(:STD)	$\mathrm{std}(I) = \sqrt{\sum_{i,j}(I(i,j)-\bar{I})^2}$	95th percentile(:95TH)	$I_{0.95}: \frac{\{p\|I(p)\ge I_{0.95}\}}{n_1 n_2} = 5\%$
Entropy(:ETP)	$\sum(-p_i \log_2 p_i),\ p_i = \frac{\|\{p\|a_i \le I(p) \le a_{i+1}\}\|}{n_1 n_2}$	95th mean(:95THM)	$I_{0.95\mathrm{mean}} = \frac{\sum_{I(p)\ge I_{0.95}} I(p)}{\|\{p\|I(p)\ge I_{0.95}\}\|}$

extracted from a preconstructed GLCM. Given the image f, the offset length l, and the angle θ, the co-occurrence matrix $G = (g(i,j))$ is defined as

$$g(i,j) = |\{(x_1,y_1),(x_2,y_2)|\ f(x_1,y_1) = i,\ f(x_2,y_2) = j,\ x_2 - x_1 = l|\cos\theta|,\ y_2 - y_1 = l|\sin\theta|\}|.$$

The size of the GLCM is decided by the number of gray levels within the image f. In all our experiments, the number of histogram bins, commonly chosen as a power of 2, was set to a fixed value of 128, based on previous studies. Parameters associated with the GLCM include the offset length l and the offset direction θ. These two parameters decide the searching direction and distance between two pixels with a given spatial relationship in image intensity. The offset length l was set equal to 10, to avoid biases in our computation from inherent physics acquisition parameters, as shown in our prior studies. To extract the features as orientation-invariant, features were calculated along all four directions of angular degree θ equal to 0°, 45°, 90°, and 135° and were then averaged for any subsequent calculations. The definitions of the seven co-occurrence features evaluated in our study are summarized in Table IV.

Energy describes the uniformity/homogeneity of the texture in the image. Entropy measures the amount of randomness of entries in GLCM, and in general, homogeneous image has low entropy and vice versa. Inverse difference moment and inertia are oppositely associated, i.e., images with coarser texture tend to have higher inverse difference moment but lower inertia. Correlation and Haralick correlation both measure the image complexity. Compared with correlation, the Haralick correlation responds stronger to the complexity. Cluster shade is related to the GLCM symmetry.

3. Run-length texture features

Run-length texture features are also used to describe the spatial relationship between pixels, and specifically, as they capture the continuous patterns (i.e., "runs") of image intensity. The features are defined based on the gray-level run-length matrix,

$$P = (p(i,j,\theta)),\ i = 1,\ldots,M,\ j = 1,\ldots,N,\ \theta = \{0°,45°,90°,135°\}$$

where $p(i,j,\theta)$ is the total number of occurrences of gray-level runs of length j at the intensity value i along the direction of θ. M is the level of image intensity and N is the range of run-length.

The run-length features capture the coarseness and complexity of a given image. Homogeneous images tend to have high long-run emphasis, low short-run emphasis, low gray-level nonuniformity, low run-length nonuniformity, and low run percentage. If a homogeneous region has low gray level, this region will have a high low gray-level run emphasis and

TABLE IV. Co-occurrence features.

Name(:notation)	Definition
Energy(:ENG)	$\sum_{(i,j)} g(i,j)^2$
Entropy(:ETP)	$-\sum_{(i,j)\|g(i,j)\ne 0} g(i,j)\log_2 g(i,j)$
Inverse difference moment(:IDM)	$\sum_{(i,j)} \frac{1}{1+(i-j)^2} g(i,j)$
Inertia(:INT)	$\sum_{(i,j)} (i-j)^2 g(i,j)$
Correlation(:COR)	$\sum_{(i,j)} \frac{(i-\mu)(j-\mu)}{\sigma^2} g(i,j)$
Haralick correlation(:HCOR)	$\sum_{(i,j)} \frac{ijg(i,j)-\mu_t^2}{\sigma_t^2}$
Cluster shade(:CSD)	$\sum_{(i,j)} ((i-\mu)+(j-\mu))^3 g(i,j)$

Notation:
$\mu_t = \frac{1}{M}\sum_{i,j} g(i,j),\ \sigma_t = \sum_i (\sum_j g(i,j) - \mu_t)^2,$
$\mu = \sum_{(i,j)} i \cdot g(i,j) = \sum_{(i,j)} j \cdot g(i,j),\ \sigma = \sum_{(i,j)} (i-\mu)^2 \cdot g(i,j) = \sum_{(i,j)} (j-\mu)^2 \cdot g(i,j).$

TABLE V. Run length features.

Name(:notation)	Definition
Short run emphasis(:SRE)	$\frac{1}{n_r}\sum_{i=1}^{M}\sum_{j=1}^{N}\frac{p(i,j,\theta)}{j^2}$
Long run emphasis(:LRE)	$\frac{1}{n_r}\sum_{i=1}^{M}\sum_{j=1}^{N}p(i,j,\theta)\cdot j^2$
Gray-level nonuniformity(:GLN)	$\frac{1}{n_r}\sum_{i=1}^{M}(\sum_{j=1}^{N}p(i,j,\theta))^2$
Run-length nonuniformity(:RLN)	$\frac{1}{n_r}\sum_{j=1}^{N}(\sum_{i=1}^{M}p(i,j,\theta))^2$
Run percentage(:RP)	n_r/n_p
Low gray-level run emphasis(:LGRE)	$\frac{1}{n_r}\sum_{i=1}^{M}\sum_{j=1}^{N}\frac{p(i,j,\theta)}{i^2}$
High gray-level run emphasis(:HGRE)	$\frac{1}{n_r}\sum_{i=1}^{M}\sum_{j=1}^{N}p(i,j,\theta)\cdot i^2$

n_r: total number of runs; n_p: total number of pixels

low high gray-level run emphasis. To generate orientation-invariant features, we also compute run-length features along four directions and average them.

4. Structure Features

a. LBP features

LBP features are designed to capture relations of a central pixel and its neighborhood pixels. In this study, the definition of LBP is based on the uniform distribution of neighborhood pixels. The LBP value at the central pixel (x_c,y_c) for image f is defined as:

$$LBP_{P,R}(x_c,y_c)=\sum_{p=0}^{P-1}s(g_p-g_c)2^P,$$
$$g_c=f(x_c,y_c),\ g_p=f(x_p,y_p),$$
$$p=0,\ldots,P-1.s(x)=1,\ x\geq 0;\ s(x)=0,\ x<0,$$
$$(x_p,y_p)=\left(x_c+R\cos\left(\frac{2\pi p}{P}\right),\ y_c-R\sin\left(\frac{2\pi p}{P}\right)\right).$$

The parameters used to define LBP features include the number of neighborhood pixel P and the radius of the neighborhood R, where R defines the size of the neighborhood, and P decides the number of pixels used within the given neighborhood. Common choices of R in previous studies include 1, 2, and 3 pixels. Here, according to the default definition, these parameters are set to $P=8$, $R=1$, as shown in Fig. 8.

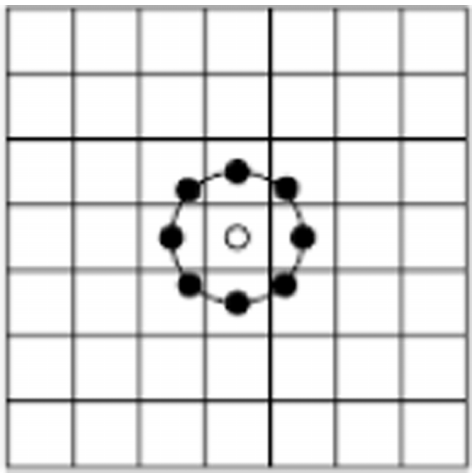

FIG. 8. Uniform distribution of LBP neighborhood ($P=8, R=1$).

b. Box-counting fractal dimension (FD)

Box-counting fractal dimension (FD) is a measure of the self-similarity in the pattern of the given image and defined as

$$d_{\mathrm{BC}}=-\lim_{\varepsilon\to 0}\frac{\ln N(r,A)}{\ln r}.$$

Here, A is a given bounded set, r is the side length of box, and $N(r,A)$ is the minimum number of nonadjacent boxes needed to cover the set A. In our study, the set A denotes the breast region.

c. Edge enhancement index (EEI)

Edge enhancement index (EEI) is used to capture inherent geometric information, especially for flow-like structures. The presence of flow-like structures within breast tissues implies that EEI might be appropriate for characterizing structural properties of the parenchymal pattern. Given an image f, EEI is defined as

$$E_\sigma(f)=\left(\frac{\lambda_1-\lambda_2}{\lambda_1+\lambda_2+\eta}\right)^2. \tag{A1}$$

Here, λ_1, λ_2 with $\lambda_1>\lambda_2$ are eigenvalues of the diffusion tensor matrix D defined as

$$D=\frac{1}{(\partial_x f_\sigma)^2+(\partial_y f_\sigma)^2}\times\begin{bmatrix}c_1(\partial_x f_\sigma)^2+c_2(\partial_y f_\sigma)^2 & (c_2-c_1)\partial_x f_\sigma\partial_y f_\sigma\\ (c_2-c_1)\partial_x f_\sigma\partial_y f & c_1(\partial_y f_\sigma)^2+c_2(\partial_x f_\sigma)^2\end{bmatrix},$$
$$f_\sigma=f*G_\sigma,\ c_2=e^{-((\partial_x f_\sigma)^2+(\partial_y f_\sigma)^2)/k^2},\ c_1=\frac{1}{5}c_2.$$

In general, when $\lambda_1\approx\lambda_2, \mathrm{E}_\sigma\approx 0$, and when $\lambda_1\gg\lambda_2, \mathrm{E}_\sigma\approx 1$, and η is an empirical normalizing factor set equal to 10 for this study. The parameter evaluated in our study is the Gaussian kernel size σ. Gaussian smoothing (i.e., $f*G_\sigma$) is used as a common image preprocessing step to remove image noise before image analysis and the kernel size determines the degree of smoothing (i.e., the extent of image details that are preserved). In our study, the G_σ was varied from 1 to 15 pixels.

[a]Author to whom correspondence should be addressed. Electronic mail: Despina.Kontos@uphs.upenn.edu; Telephone: 215-615-0827; Fax: 215-614-0266.

[1]R. Siegel, D. Naishadham, and A. Jemal, "Cancer statistics, 2013," CA-Cancer J. Clin. **63**, 11–30 (2013).
[2]E. D. Pisano, C. Gatsonis, E. Hendrick, M. Yaffe, J. K. Baum, S. Acharyya, E. F. Conant, L. L. Fajardo, L. Bassett, C. D'Orsi, R. Jong, and M. Rebner, "Diagnostic performance of digital versus film mammography for breast-cancer screening," N. Engl. J. Med. **353**, 1773–1783 (2005).

[3]A. Fischmann, K. C. Siegmann, A. Wersebe, C. D. Claussen, and M. Muller-Schimpfle, "Comparison of full-field digital mammography and film-screen mammography: Image quality and lesion detection," Br. J. Radiol. **78**, 312–315 (2005).
[4]P. Skaane and A. Skjennald, "Screen-film mammography versus full-field digital mammography with soft-copy reading: Randomized trial in a population-based screening program–The Oslo II study," Radiology **232**, 197–204 (2004).
[5]P. Skaane, "Studies comparing screen-film mammography and full-field digital mammography in breast cancer screening: Updated review," Acta Radiol. **50**, 3–14 (2009).
[6]J. N. Wolfe, "Risk for breast cancer development determined by mammographic parenchymal pattern," Cancer **37**, 2486–2492 (1976).
[7]J. N. Wolfe, "Breast patterns as an index of risk for developing breast cancer," Am. J. Roentgenol. **126**, 1130–1137 (1976).
[8]M. Nielsen, G. Karemore, M. Loog, J. Raundahl, N. Karssemeijer, J. D. Otten, M. A. Karsdal, C. M. Vachon, and C. Christiansen, "A novel and automatic mammographic texture resemblance marker is an independent risk factor for breast cancer," Cancer Epidemiol. **35**, 381–387 (2011).
[9]G. Torres-Mejia, B. De Stavola, D. S. Allen, J. J. Perez-Gavilan, J. M. Ferreira, I. S. Fentiman, and I. Dos Santos Silva, "Mammographic features and subsequent risk of breast cancer: A comparison of qualitative and quantitative evaluations in the Guernsey prospective studies," Cancer Epidemiol., Biomarkers Prev. **14**, 1052–1059 (2005).
[10]H. Li, M. L. Giger, O. I. Olopade, and L. Lan, "Fractal analysis of mammographic parenchymal patterns in breast cancer risk assessment," Acad. Radiol. **14**, 513–521 (2007).
[11]A. Manduca, M. J. Carston, J. J. Heine, C. G. Scott, V. S. Pankratz, K. R. Brandt, T. A. Sellers, C. M. Vachon, and J. R. Cerhan, "Texture features from mammographic images and risk of breast cancer," Cancer Epidemiol., Biomarkers Prev. **18**, 837–845 (2009).
[12]J. J. Heine and P. Malhotra, "Mammographic tissue, breast cancer risk, serial image analysis, and digital mammography. Part 2. Serial breast tissue change and related temporal influences," Acad. Radiol. **9**, 317–335 (2002).
[13]J. J. Heine and P. Malhotra, "Mammographic tissue, breast cancer risk, serial image analysis, and digital mammography. Part 1. Tissue and related risk factors," Acad. Radiol. **9**, 298–316 (2002).
[14]M. A. Sanders, L. Roland, and S. Sahoo, "Clinical implications of subcategorizing BI-RADS 4 breast lesions associated with microcalcification: A radiology-pathology correlation study," Breast J. **16**, 28–31 (2010).
[15]N. F. Boyd *et al.*, "Mammographic density and the risk and detection of breast cancer," N. Engl. J. Med. **356**, 227–236 (2007).
[16]L. J. Lu, T. K. Nishino, T. Khamapirad, J. J. Grady, M. H. Leonard, Jr., and D. G. Brunder, "Computing mammographic density from a multiple regression model constructed with image-acquisition parameters from a full-field digital mammographic unit," Phys. Med. Biol. **52**, 4905–4921 (2007).
[17]J. J. Heine, K. Cao, D. E. Rollison, G. Tiffenberg, and J. A. Thomas, "A quantitative description of the percentage of breast density measurement using full-field digital mammography," Acad. Radiol. **18**, 556–564 (2011).
[18]B. M. Keller, D. L. Nathan, Y. Wang, Y. Zheng, J. C. Gee, E. F. Conant, and D. Kontos, "Estimation of breast percent density in raw and processed full field digital mammography images via adaptive fuzzy c-means clustering and support vector machine segmentation," Med. Phys. **39**, 4903–4917 (2012).
[19]J. Li, L. Szekely, L. Eriksson, B. Heddson, A. Sundbom, K. Czene, P. Hall, and K. Humphreys, "High-throughput mammographic-density measurement: A tool for risk prediction of breast cancer," Breast Cancer Res. **14**, R114 (12pp.) (2012).
[20]J. J. Heine, C. G. Scott, T. A. Sellers, K. R. Brandt, D. J. Serie, F. F. Wu, M. J. Morton, B. A. Schueler, F. J. Couch, J. E. Olson, V. S. Pankratz, and C. M. Vachon, "A novel automated mammographic density measure and breast cancer risk," JNCI, J. Natl. Cancer Inst. **104**, 1028–1037 (2012).
[21]I. T. Gram, E. Funkhouser, and L. Tabar, "The tabar classification of mammographic parenchymal patterns," Eur. J. Radiol. **24**, 131–136 (1997).
[22]Z. Huo, M. L. Giger, O. I. Olopade, D. E. Wolverton, B. L. Weber, C. E. Metz, W. Zhong, and S. A. Cummings, "Computerized analysis of digitized mammograms of BRCA1 and BRCA2 gene mutation carriers," Radiology **225**, 519–526 (2002).
[23]H. Li, M. L. Giger, O. I. Olopade, A. Margolis, L. Lan, and M. R. Chinander, "Computerized texture analysis of mammographic parenchymal patterns of digitized mammograms," Acad. Radiol. **12**, 863–873 (2005).
[24]S. Petroudi, T. Kadir, and M. Brady, "Automatic classification of mammographic parenchymal patterns: A statistical approach," in *Proceedings of the 25th Annual International Conference of the IEEE Engineering in Medicine and Biology Society*, Vol. 1 (IEEE, Cancun, Mexico, 2003), pp. 798–801.
[25]J. Wei, H. P. Chan, Y. T. Wu, C. Zhou, M. A. Helvie, A. Tsodikov, L. M. Hadjiiski, and B. Sahiner, "Association of computerized mammographic parenchymal pattern measure with breast cancer risk: A pilot case-control study," Radiology **260**, 42–49 (2011).
[26]Y. Yuan, M. L. Giger, H. Li, and C. Sennett, "Correlative feature analysis on FFDM," Med. Phys. **35**, 5490–5500 (2008).
[27]J. J. Heine and R. P. Velthuizen, "Spectral analysis of full field digital mammography data," Med. Phys. **29**, 647–661 (2002).
[28]L. Haberle, F. Wagner, P. A. Fasching, S. M. Jud, K. Heusinger, C. R. Loehberg, A. Hein, C. M. Bayer, C. C. Hack, M. P. Lux, K. Binder, M. Elter, C. Munzenmayer, R. Schulz-Wendtland, M. Meier-Meitinger, B. R. Adamietz, M. Uder, M. W. Beckmann, and T. Wittenberg, "Characterizing mammographic images by using generic texture features," Breast Cancer Res. **14**, R59 (12pp.) (2012).
[29]M. Tuceryan and A. K. Jain, "Texture analysis," in *Handbook of Pattern Recognition and Computer Vision* (World Scientific, Singapore, 1993), pp. 235–276.
[30]B. Julesz, "Textons, the elements of texture perception, and their interactions," Nature **290**, 91–97 (1981).
[31]M. H. Bharati, J. J. Liu, and J. F. MacGregor, "Image texture analysis: Methods and comparisons," Chemom. Intell. Lab. Syst. **72**, 57–71 (2004).
[32]H. Tamura, S. Mori, and T. Yamawaki, "Textural features corresponding to visual perception," IEEE Trans. Syst., Man, Cybern. **8**, 460–473 (1978).
[33]Y. Zheng, B. Keller, Y. Wang, N. Tustison, G. Song, P. Bakic, A. Maidment, E. Conant, J. Gee, and D. Kontos, "A fully-automated software pipeline for parenchymal pattern analysis in digital breast images: Toward the translation of imaging biomarkers in routine breast cancer risk assessment," in *Quantitative Imaging Reading Room, the 97th Scientific Assembly and Annual Meeting of the Radiological Society of North America (RSNA)* (RNSA, Chicago, IL, 2011).
[34]Y. Zheng, Y. Wang, B. M. Keller, E. Conant, J. C. Gee, and D. Kontos, "A fully-automated software pipeline for integrating breast density and parenchymal texture analysis for digital mammograms: Parameter optimization in a case-control breast cancer risk assessment study," Proc. SPIE **8670**, 86701B (2013).
[35]Z. Chen and R. Zwiggelaar, "A modified fuzzy c-means algorithm for breast tissue density segmentation in mammograms," in *10th IEEE International Conference on Information Technology and Applications in Biomedicine (ITAB)* (IEEE, Corfu, 2010), pp. 1–4.
[36]B. S. Garra, B. H. Krasner, S. C. Horii, S. Ascher, S. K. Mun, and R. K. Zeman, "Improving the distinction between benign and malignant breast lesions: The value of sonographic texture analysis," Ultrason. Imaging **15**, 267–285 (1993).
[37]R. M. Haralick, K. Shanmugam, and I. H. Dinstein, "Textural features for image classification," IEEE Trans. Syst., Man, Cybern. **SMC-3**, 610–621 (1973).
[38]M. M. Galloway, "Texture analysis using gray level run lengths," Comput. Graphics Image Process. **4**, 172–179 (1975).
[39]H. Li, M. L. Giger, Z. Huo, O. I. Olopade, L. Lan, B. L. Weber, and I. Bonta, "Computerized analysis of mammographic parenchymal patterns for assessing breast cancer risk: Effect of ROI size and location," Med. Phys. **31**, 549–555 (2004).
[40]C. B. Caldwell, S. J. Stapleton, D. W. Holdsworth, R. A. Jong, W. J. Weiser, G. Cooke, and M. J. Yaffe, "Characterisation of mammographic parenchymal pattern by fractal dimension," Phys. Med. Biol. **35**, 235–247 (2000).
[41]T. Ojala, M. Pietikainen, and T. Maenpaa, "Multiresolution gray-scale and rotation invariant texture classification with local binary patterns," IEEE Trans. Pattern Anal. Mach. Intell. **24**, 971–987 (2002).
[42]J. Weickert, "Coherence-enhancing diffusion filtering," Int. J. Comput. Vision **31**, 111–127 (1999).
[43]G. Karemore, S. Brandt, J. Sporring, and M. Nielsen, "Anisotropic diffusion tensor applied to temporal mammograms: An application to breast cancer risk assessment," in *2010 Annual International Conference of the IEEE Engineering in Medicine and Biology Society* (IEEE, Buenos Aires, 2010), pp. 3178–3181.

[44]A. Oliver, J. Freixenet, R. Marti, J. Pont, E. Perez, E. R. Denton, and R. Zwiggelaar, "A novel breast tissue density classification methodology," IEEE Trans. Inf. Technol. Biomed. **12**, 55–65 (2008).
[45]Y. Wang, B. M. Keller, Y. Zheng, R. J. Acciavatti, J. C. Gee, A. D. Maidment, and D. Kontos, "Texture feature standardization in digital mammography for improving generalizability across devices," Proc. SPIE **8670**, 86701B (2013).
[46]Y. Wang, B. Keller, Y. Zheng, R. Acciavatti, J. Gee, A. Maidment, and D. Kontos, "A phantom study for assessing the effect of different digital detectors on mammographic texture features," in *Breast Imaging*, Lecture Notes in Computer Science Vol. 7361 (Springer, Berlin, Heidelberg, 2012), pp. 604–610.
[47]B. M. Keller, A. Oustimov, Y. Wang, J. Chen, R. Acciavatti, Y. Zheng, S. Ray, J. C. Gee, A. D. A. Maidment, and D. Kontos, "Parenchymal texture analysis in digital mammography: Robust texture feature identification and equivalence across devices," J. Med. Imaging **2**, 024501 (2015).
[48]N. Sarkar and B. B. Chaudhuri, "An efficient differential box-counting approach to compute fractal dimension of image," IEEE Trans. Syst., Man, Cybern. **24**, 115–120 (1994).
[49]M. Stone, "An asymptotic equivalence of choice of model by cross-validation and Akaike's criterion," J. R. Stat. Soc. Ser. B (Methodological) **39**, 44–47 (1977).
[50]H. Liu and H. Motoda, *Computational Methods of Feature Selection* (Chapman and Hall/CRC, Boca Raton, FL, 2007).
[51]C. E. Metz, B. A. Herman, and J. H. Shen, "Maximum likelihood estimation of receiver operating characteristic (ROC) curves from continuously-distributed data," Stat. Med. **17**, 1033–1053 (1998).
[52]E. R. Delong, D. M. Delong, and D. L. Clarke-Pearson, "Comparing the areas under two or more correlated receiver operating characteristic curves: A nonparametric approach," Biometrics **44**, 837–845 (1988).
[53]See supplementary material at http://dx.doi.org/10.1118/1.4921996 for the area under the curve (AUC) of each lattice-based texture feature at all different parameter settings .
[54]N. F. Boyd, G. A. Lockwood, J. W. Byng, D. L. Tritchler, and M. J. Yaffe, "Mammographic densities and breast cancer risk," Cancer Epidemiol., Biomarkers Prev. **7**, 1133–1144 (1998).
[55]J. A. Tice, S. R. Cummings, R. Smith-Bindman, L. Ichikawa, W. E. Barlow, and K. Kerlikowske, "Using clinical factors and mammographic breast density to estimate breast cancer risk: Development and validation of a new predictive model," Ann. Intern. Med. **148**, 337–347 (2008).
[56]W. He, I. Muhimmah, E. R. Denton, and R. Zwiggelaar, "Mammographic segmentation based on texture modelling of tabar mammographic building blocks," in *Digital Mammography* (Springer, New York, NY, 2008), pp. 17–24.
[57]I. T. Jolliffe and L. A. Duhring Fund, *Principal Component Analysis*, 2nd ed. (Springer, New York, 2004).
[58]Y. Zheng, H. Wang, J. Wu, J. Gao, and J. C. Gee, "Multiscale analysis revisited: Detection of drusen and vessel in digital retinal images," in *IEEE International Symposium on Biomedical Imaging: From Nano to Macro* (IEEE, Chicago, IL, 2011), pp. 689–692.
[59]P. W. Jones and T. M. Le, "Local scales and multiscale image decompositions," Appl. Comput. Harmon. Anal. **26**, 371–394 (2009).
[60]A. Eng, Z. Gallant, J. Shepherd, V. McCormack, J. Li, M. Dowsett, S. Vinnicombe, S. Allen, and I. Dos-Santos-Silva, "Digital mammographic density and breast cancer risk: A case inverted question mark control study of six alternative density assessment methods," Breast Cancer Res. **16**, 439 (12pp.) (2014).
[61]E. Amir, O. C. Freedman, B. Seruga, and D. G. Evans, "Assessing women at high risk of breast cancer: A review of risk assessment models," JNCI, J. Natl. Cancer Inst. **102**, 680–691 (2010).